*Graphical Abstract

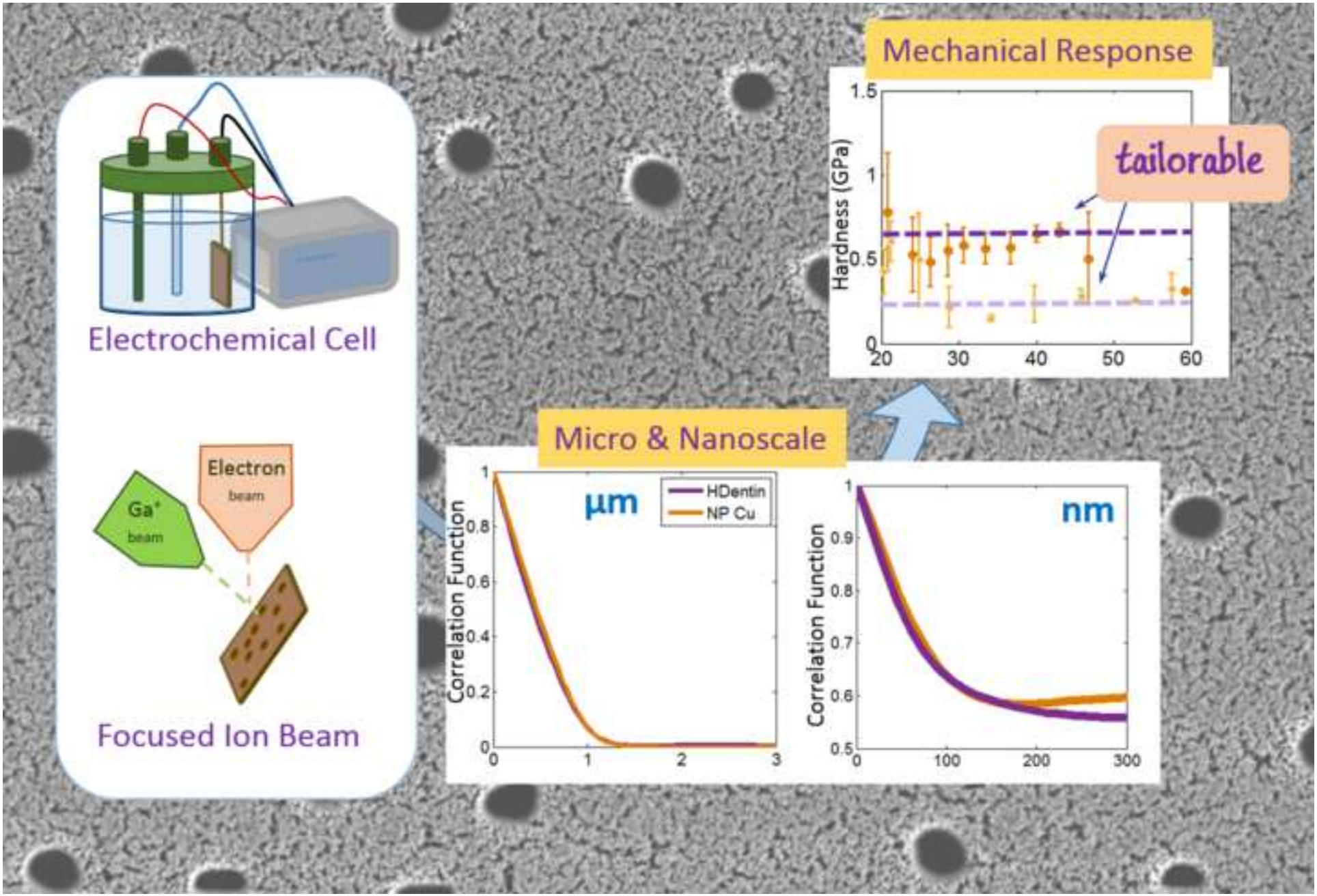

Structure and mechanical behavior of dentin-inspired nanoporous copper

*Timothy Ibru[1], Sarah Violante[1], Elsa Vennat[2], Chloé Arson[3] and Antonia Antoniou[1]**

[1] The Woodruff School of Mechanical Engineering, Georgia Institute of Technology, Atlanta, GA 30332

[2] Centrale-Supélec - Laboratoire MSSMat, Paris, France

3 Civil and Environmental Engineering, Georgia Institute of Technology, Atlanta, GA 30332

*Corresponding author: antonia.antoniou@me.gatech.edu

Keywords: nanoporous, dentin, structure, property, modulus, hardness.

Abstract Dentin possesses a hierarchical porous structure with varying cross-scale morphology and characteristic lengths ranging from nanometers to micrometers. NP Copper is fabricated with nano-sized and micron-sized features that mimic dentin's morphology. NP Copper Young's modulus, hardness, and plastic Poisson's ratio are shown to be in the range characteristic of dentin. This correspondence in properties may allow use of NP metals to advance tooth restoration techniques, for example by using NP metals as model systems to study infiltration of dentin with resins. Moreover, the multi-scale porosity may inspire design of 3D catalysts with efficient reactant mass transport through the catalyst volume.

Main Text:

Biological material properties have evolved over extended periods of time to suit specific functions. Taking clues from Nature often enables scientists to take unusual shortcuts, yielding materials with enhanced properties. We report on one such example of a biologically inspired material system, nanoporous(NP) Copper which has morphological structure and physical properties close to those of dentin, a hard tissue that is part of the tooth.

NP metals consist of a 3D hierarchical network of ligaments with characteristic scale lengths ~2-100nm[1]. These structural elements can have internal structure, e.g. ligaments may consist of nanosized grains, twin boundaries, etc.[2-7]. Many unusual NP metal properties as well as many applications are ultimately related to their extremely high surface to volume ratio. NP metals have been used in a diverse range of applications, such as catalysts[8-11], electrochemical electrodes[12, 13], interconnect components[14], actuators [15-17] and sensors[18-20].

Dentin is a natural porous material found in teeth. Encased in enamel, the dentinal tissue[21] has a hierarchical structure with characteristic scale sizes spanning micro- to nano- scales (see Fig. 1). At the microscale, dentin consists of hollow cylinders called tubules, which traverse the entire height of the dentin from the pulp to the enamel and are filled with a fluid similar to plasma. The orientation, diameter and density of the tubules changes across the entire perimeter of the tooth[22]. At the nanoscale, dentin consists of collagen fibrils(CF) and hydroxyapatite crystals(HA)[22]. Dentin's mechanical properties, similar to other natural materials, range between those of dense metals and polymers, overlapping with NP metal properties. Dentin has relatively high fracture toughness (1-3MPa$\sqrt{m}$)[23, 24] and moderate stiffness (7-20GPa)[25] that strongly depends on tubule distribution and hydration. Dentin possesses excellent fatigue life and

has distinct and complementary properties compared to enamel, the exterior hard tissue of the tooth, so that cracks initiating from the brittle enamel surface may be arrested at the interface with dentin[26].

The remarkable similarity in the nanoscale structure and mechanical properties between NP metals and dentin invites further exploration. In particular, we will demonstrate that the nanoscale and microscale porosity of dentin can be replicated in NP metals, yielding a structure morphologically identical to dentin. Such structures are of great interest for several reasons. First, NP metals could potentially be used as part of tooth restoration treatments, or even as dentin analogs, to study infiltration of resins into dentin. Typical tooth restoration procedures require that dentin be demineralized and infiltrated with a resin composite. The hybrid layer at the interface between resin and healthy dentin is the main cause of failure of tooth restorations[27, 28] and the optimization of its properties is highly desirable. At the same time, biological samples are unique, non-reproducible, environmentally sensitive, and require sophisticated testing protocols[29], leading to substantial uncertainty in the experiments. An "equivalent" system, such as NP Copper, with physical properties close to those of dentin and that can be fabricated relatively easily and reproducibly, could help design adaptable resin-based tooth restorations thus having a significant impact on public health[30]. It is also notable that other NP metal systems e.g.,NP Silver or NP Copper Oxide, possess antimicrobial properties[31, 32]. Incorporation of such oxide nanoparticles into dental resins has recently been suggested[33].

More generally, replicating dentin's hierarchical porosity may substantially aid liquid or gas reactant transport through the 3D structure of NP metals. The dentin porous network is naturally optimized for fluid and biological signal transmission through odontoblastic processes[34]. This natural optimization may inform the design of highly efficient 3D electrodes and catalysts[35],

which could maintain mechanical integrity under cyclic thermo-mechanical loads, similarly to how dentin plays a key role in maintaining mechanical integrity of teeth under cyclic loads. In such applications, the key issue, irrespective of the type of fluid, is whether accessibility of active sites through the volume is possible.

NP metals are controllably fabricated by a three-step process involving synthesis of a precursor alloy that is then preferentially etched leaving a three dimensional network of nanosized ligaments and pores. Both NP metal foils and bars can be fabricated. The precursor alloy type, the composition of the precursor, as well as the etchant type and the dealloying rate impact the eventual nanoporous metal structure[36-40]. The nanocrystalline NP metals[7, 41] that we synthesize originate from dealloying amorphous ribbons[2-7].

Nanoporous Copper (NP Cu) was fabricated after controlled etching of Copper Silicide amorphous alloy thin film. Two precursor alloys were used: $Cu_{0.25}Si_{0.75}$ and $Cu_{0.41}Si_{0.59}$ (atom %) as characterized by X-ray photoelectron spectroscopy (XPS) and were sputter deposited onto a silicon wafer under 100V bias. The precursor alloys were etched in 3% HF in deionized water under an applied potential of $V=-0.3V$ with respect to a standard calomel electrode (SCE). The potential was applied for 100s, after which the samples were rinsed in deionized water and air-dried. The composition after dealloying, the residual stress state of the $Cu_{0.41}Si_{0.59}$ (atom %) precursor alloy and the presence of nanocrystallites within the ligaments are described in a prior publication[41]. Some of the NP Copper samples were exposed in the electrolyte up to 60 minutes to increase the thickness of the ligaments.

After etching, the samples were imaged using the FEI NovaNanolab 200 FIB/Scanning Electron Microscope (SEM) and top views and through thickness views were obtained. The SEM images

were used to obtain the film thickness, ligament dimensions and relative density (solid mass fraction) using Image J[42].

Dentin from a third molar was cut in a plane perpendicular to the tubules, in the coronal part of the tooth. The sectioned dentin was subsequently progressively polished up to a micron size finish using a 1μm diamond suspension. The sample was then dehydrated by exposing it in an ethanol solution of increasing concentration and placed on a brass holder using silver paste to limit charging during imaging. The obtained sample was then imaged using an SEM(Helios 660, Zeiss) at 2kV and 0.2nA at a working distance of 2.3mm using back-scattered electron imaging. Different magnifications of the tubules were obtained. Demineralized dentin was obtained by removal of the HA using a protocol described in Ref.[43]. The demineralized dentin was imaged in SEM using a similar protocol.

The tubules were formed in some of the precursor alloy samples using a FEI NovaNanolab 200 FIB/SEM where a beam of Gallium ions is used to etch away features on the sample surface. As seen from the schematic of Fig. 1(a) and the SEM images of Fig. 1(b) the tubules have a circular cross-section perpendicular to the tooth perimeter; they are long elongated cylinders in the plane connecting the enamel and tooth root. The tubules created with the FIB on nanoporous copper reflect the exact pattern from the SEM images of the dentin sample. A mask was created by thresholding SEM images of dentin to capture the tubules' spacing and size. Using "xT microscope control", the user interface for the Nova 200 NanoLab-DualBeamTM-SEM/FIB, the tubules were etched on NP Copper to mimic the actual dentin tubule spacing and size. The ion beam milling was performed at 30kV with a beam current of 0.5nA.

The structure of the dentin samples (healthy and demineralized) as well as the NP Copper sample were compared by thresholding the SEM images using a triangle algorithm[44] implemented in Image J[42]. Any noise in the images was reduced using a median filter with a 10-16 pixel radius depending on magnification. The resulting binarized images for all samples were used to calculate a two-point correlation function defined as $C(r) = \langle I(\mathbf{x})I(\mathbf{x}+\mathbf{r})\rangle$, where I denotes the image intensity at location **x**, and $\langle ... \rangle$ denotes averaging over all locations **x**. The features in the images were isotropic in the statistical sense so the correlation function has only a dependence on the radial distance $r = |\mathbf{r}|$[45, 46]. The correlation function was calculated at two different magnifications to highlight the nanoscale structure of the dentin and NP Copper as well as the micron sized scale structure, with the presence of tubules.

Mechanical properties of NP copper were obtained using Berkovich nanoindentation[41]. For a small subset of samples, frustum indentation was also performed[47]. The samples used in the mechanical tests were synthesized under the same exact conditions as those with the fabricated FIB tubules. Berkovich nanoindentation with a ~150μm sized tip was performed using a Hysitron nanoindenter. Tip area calibrations were performed using standard protocols: properties of known materials (e.g. aluminum) were verified using the standard Oliver and Pharr method[48] prior to testing of NP Copper. For each sample, 25 indents 40μm apart were performed up to 2000 μN. Measurements obtained with indentation depths higher than a single pore (>30-50 nm) and smaller than 30% of the film thickness were averaged to obtain a single value for the hardness, H, where $H=F_{max}/A_{contact}$, is the peak indent force divided by the contact area. In addition, the reduced modulus, E_r, was obtained from the unloading indentation curve. The reduced modulus and hardness values were plotted as a function of ligament thickness for each sample. A 3-point

moving average was calculated for the modulus and hardness measurements as a function of ligament thickness.

Scanning Electron Microscopy (SEM) images of healthy dentin tubules are shown in Fig. 2(a)-(b). Figures 2(c)-(d) show the tubule spacing and size as replicated in NP Copper using a Focused Ion Beam (FIB). The NP Copper sample has ~35nm sized ligament thickness and was obtained by controlled dealloying of $Cu_{0.41}Si_{0.59}$(atom %) in Hydrofluoric acid(HF). The tubules were fabricated according to the protocol described in the Methods section and the SEM images were taken at the same magnification as the dentin images. As shown, the exact same tubule arrangement can be easily replicated in the NP Copper sample. In appearance, NP Copper has open porosity similar to demineralized dentin. Healthy dentin on the other hand, consists of intermixed collagen and hydroxyapatite crystals (HA)[22, 49] (Fig. 1).

The correlation function is shown with radial distance in Fig. 3(a) at the microscale and in Fig. 3(b) at the nanoscale. The correlation function is obtained by thresholding the SEM images of Fig. 2 for dentin (healthy and demineralized) and NP Copper. From Fig. 3(a), the probability of finding identical features at the microscale decreases with increasing radial distance in the same manner for healthy dentin and NP Cu. This of course makes sense since the tubule network size and spacing in the dentin sample was designed and precisely replicated in the NP Cu sample.

Figure 3(b) shows the dependence of the correlation function on the radial distance at the nanoscale for NP Copper, healthy and demineralized dentin. The correlation function for NP Copper decreases with radial distance and reaches a plateau that corresponds to the relative mass fraction of this particular NP Copper sample (~60%). The characteristic scale for NP Copper from Fig. 3(b) is found to be 45.8nm. The characteristic scale is defined as the radial distance at a correlation

coefficient of ~0.8 which is between the plateau value (0.6) and peak (1). In a similar fashion the plateau for healthy dentin is found to be 56% and the characteristic scale is found to be 45.2nm. The plateau for demineralized dentin, from thresholding Fig. 2(c), corresponds to a solid mass fraction of 46% and a characteristic scale of 60nm. The dentin SEM images were obtained using backscattered electrons and have the advantage of being sensitive to the atomic mass. For instance, in healthy dentin made of collagen fibrils and hydroxyapatite (HA), the heavier HA crystals will appear brighter than the collagen fibrils. When healthy dentin images are thresholded, they can reveal the structure of the HA component. The correlation function plateau corresponds to the relative area of the HA component (bright field) for healthy dentin. On the other hand, since the demineralization step etches out HA, the plateau for the demineralized dentin mostly corresponds to collagen. We note that the etching process can cause shrinkage of the collagen network, which may slightly overestimate the collagen area fraction by a few percent[50]. From the plateau values of Fig. 3(b), the relative area of healthy and demineralized dentin are dual to each other since the former corresponds to the HA component area fraction and the latter to mainly collagen. The characteristic scale for demineralized dentin found from this analysis is ~60nm which is consistent with the characteristic scale of collagen measured from small-angle x-ray scattering[51].

Figure 4 shows the average hardness, H and the reduced modulus E_r as functions of ligament thickness for NP Copper generated from two different initial alloy compositions, $Cu_{0.25}Si_{0.75}$, (black symbols) and $Cu_{0.41}Si_{0.59}$ (red symbols). The blue dotted lines on both inserts show the average healthy dentin modulus with Fig. 4(a) showing the modulus variation depending on location and hydration level[25, 52] in light blue. For demineralized dentin, the modulus is in the range of 0.2-7GPa, depending on hydration level[25, 53]. The hardness of demineralized dentin (cyan dotted line) is also shown in Fig. 4(b)[25, 52]. NP Copper in the range of 30-50 nm from

$Cu_{0.25}Si_{0.75}$ has closer values to healthy dentin but it is possible to fabricate samples with features more similar to demineralized dentin. Other physical properties of NP Copper also have an overlap with dentin and are summarized in Table 1. For example, the plastic Poisson's ratio, a measure of lateral dimensional changes in a material beyond yielding, is a crucial parameter when describing the pressure sensitivity of the yield surface of a porous medium[54].

Dense solids have a plastic Poisson's ratio of 0.5; low density porous media have a plastic Poisson's ratio of ~0. The plastic Poisson's ratio of dentin was measured to be ~0.3[52]. NP metals have been reported to have a plastic Poisson's ratio of 0.2-0.3[47, 55]. The design of NP metals with nanoscale structure and mechanical properties similar to dentin, may allow for calibration of numerical models formulated to examine the mechanical response of dentin. For example, dentin stiffness models based on the homogenization scheme of Hashin[56], in which the volume distribution of peri-tubular dentin around the tubules, that is stiffer than inter-tubular dentin that is away from the tubules, is assigned a non-uniform distribution, determined from image analysis[57], may benefit from additional information coming from the mechanical response of NP Copper with FIB generated tubules.

In summary, we engineered NP Copper to have similar Young's modulus, hardness and plastic Poisson's ratio with dentin. Imparting the microscale tubule network on NP Copper via micro/nanofabrication methods in a controllable and repeatable fashion may make NP Copper an ideal model system to study properties of dentin infiltration with resin composites, which in turn may enable numerical model calibration and advance resin-based tooth restoration. Intriguingly, fabricating NP metals with a hierarchical porosity inspired by dentin may provide a path towards stable 3D catalysts with enhanced bimodal porosity, enabling enhanced transport of the reactant fluid through the structure. This may help overcome the well-known limitation that the interior

surface area of NP metals is not readily accessible for traditional structures[58]. While there are several proposed methods for introducing a bimodal porosity for catalysis applications[59, 60] including fractal inspired structures[61], dentin-inspired bimodal porosity may help maintain mechanical properties while enhancing transport.

Acknowledgements

Funding for this work was made possible through an REU grant and NSF CAREER No.1351705. Dr. Arson received funding from Université Paris-Saclay (bourse d'Alembert: Micro-macro mechanical modeling of teeth with cavities restored by resin-based techniques, Arson and Vennat, 2017-2018). This work was performed, in part, at the Center for Integrated Nanotechnologies, an Office of Science User Facility operated for the U.S. Department of Energy (DOE) Office of Science by Los Alamos National Laboratory (Contract 89233218CNA000001) and Sandia National Laboratories (Contract DE-NA-0003525).

References

[1] Y. Ding, Y.J. Kim, J. Erlebacher. Advanced Materials 16 (2004) 1897-1900.
[2] T. Aburada, J.M. Fitz-Gerald, J.R. Scully. Corrosion Science 53 (2011) 1627-1632.
[3] A. Antoniou, D. Bhattacharrya, J.K. Baldwin, P. Goodwin, M. Nastasi, S.T. Picraux, A. Misra. Applied Physics Letters 95 (2009).
[4] Z. Dan, F. Qin, Y. Sugawara, I. Muto, N. Hara. Intermetallics 29 (2012) 14-20.
[5] R. Liu, S. Zheng, J. Kevin Baldwin, M. Kuthuru, N. Mara, A. Antoniou. Applied Physics Letters 103 (2013) -.
[6] Z. Wang, J. Liu, C. Qin, L. Liu, W. Zhao, A. Inoue. Intermetallics 56 (2015) 48-55.
[7] R. Liu, J. Gruber, D. Bhattacharyya, G.J. Tucker, A. Antoniou. Acta Materialia 103 (2016) 624-632.
[8] Y. Ding, M. Chen. MRS bulletin 34 (2009) 569-576.
[9] T. Fujita, P. Guan, K. McKenna, X. Lang, A. Hirata, L. Zhang, T. Tokunaga, S. Arai, Y. Yamamoto, N. Tanaka. Nat. Mater. 11 (2012) 775.
[10] R. Kraehnert, E. Ortel, B. Paul, B. Eckhardt, M. Kanis, R. Liu, A. Antoniou. Catalysis Science & Technology 5 (2015) 206-216.
[11] T. Juarez, J. Biener, J. Weissmüller, A.M. Hodge. Advanced Engineering Materials 19 (2017) 1700389.
[12] T. Wada, J. Yamada, H. Kato. Journal of Power Sources 306 (2016) 8-16.
[13] E. Detsi, X. Petrissans, Y. Yan, J.B. Cook, Z. Deng, Y.-L. Liang, B. Dunn, S.H. Tolbert. Physical Review Materials 2 (2018) 055404.
[14] K. Mohan, N. Shahane, R. Liu, V. Smet, A. Antoniou. JOM (2018).
[15] H.J. Jin, J. Weissmüller. Advanced engineering materials 12 (2010) 714-723.
[16] J. Zhang, Q. Bai, Z. Zhang. Nanoscale 8 (2016) 7287-7295.
[17] J. Biener, A. Wittstock, L. Zepeda-Ruiz, M. Biener, V. Zielasek, D. Kramer, R. Viswanath, J. Weissmüller, M. Bäumer, A. Hamza. Nat. Mater. 8 (2009) 47.
[18] Y. Li, Y. Liu, J. Liu, J. Liu, H. Tang, C. Cao, D. Zhao, Y. Ding. Scientific reports 5 (2015) 7699.
[19] R. Song, L. Zhang, F. Zhu, W. Li, Z. Fu, B. Chen, M. Chen, H. Zeng, D. Pan. Advanced Materials Interfaces 5 (2018) 1800332.
[20] S. Sen, D. Liu, G.T.R. Palmore. Acs Catalysis 4 (2014) 3091-3095.
[21] L.W. Boushell, J.R. Sturdevant. Sturdevant's Art & Science of Operative Dentistry (2014) 1-40.
[22] E. Vennat. Étude expérimentale et numérique de l'infiltration de la dentine déminéralisée en surface par des résines composites. Châtenay-Malabry, Ecole centrale de Paris, 2009.
[23] C. Montoya, D. Arola, E. Ossa. Archives of oral biology 67 (2016) 9-14.
[24] V. Imbeni, J. Kruzic, G. Marshall, S. Marshall, R. Ritchie. Nat. Mater. 4 (2005) 229.
[25] L.E. Bertassoni. Dental Materials 33 (2017) 637-649.
[26] M. Yahyazadehfar, J. Ivancik, H. Majd, B. An, D. Zhang, D. Arola. Applied mechanics reviews 66 (2014) 030803.
[27] M. Toledano, F.S. Aguilera, S. Sauro, I. Cabello, E. Osorio, R. Osorio. Dental Materials 30 (2014) e169-e188.
[28] P. Spencer, Q. Ye, J. Park, E.M. Topp, A. Misra, O. Marangos, Y. Wang, B.S. Bohaty, V. Singh, F. Sene. Annals of biomedical engineering 38 (2010) 1989-2003.
[29] D.C. Sarrett. Dental Materials 21 (2005) 9-20.

[30] J.W. van Dijken, U. Pallesen. dental materials 27 (2011) 150-156.
[31] I.M. Hamouda. Journal of biomedical research 26 (2012) 143.
[32] Q. Yu, Z. Wu, H. Chen. Acta Biomaterialia 16 (2015) 1-13.
[33] A. Shrestha, S.-W. Fong, B.-C. Khoo, A. Kishen. Journal of Endodontics 35 (2009) 1028-1033.
[34] H. Magloire, M.L. Couble, B. Thivichon-Prince, J.C. Maurin, F. Bleicher. Journal of Experimental Zoology Part B: Molecular and Developmental Evolution 312 (2009) 416-424.
[35] C.M. Parlett, K. Wilson, A.F. Lee. Chemical Society Reviews 42 (2013) 3876-3893.
[36] J.C. Thorp, K. Sieradzki, L. Tang, P.A. Crozier, A. Misra, M. Nastasi, D. Mitlin, S.T. Picraux. Applied Physics Letters 88 (2006) 1-3.
[37] A.M. Hodge, J. Biener, J.R. Hayes, P.M. Bythrow, C.A. Volkert, A.V. Hamza. Acta Materialia 55 (2007) 1343-1349.
[38] Y. Sun, T.J. Balk. Scripta Materialia 58 (2008) 727-730.
[39] R. Liu, A. Antoniou. Scripta Materialia 67 (2012) 923-926.
[40] K. Mohan, N. Shahane, R. Liu, V. Smet, A. Antoniou. JOM 70 (2018) 2192-2204.
[41] R. Liu, S. Zheng, J.K. Baldwin, M. Kuthuru, N. Mara, A. Antoniou. Applied Physics Letters 103 (2013) 241907.
[42] M.D. Abràmoff, P.J. Magalhães, S.J. Ram. Biophotonics international 11 (2004) 36-42.
[43] E. Vennat, C. Bogicevic, J.-M. Fleureau, M. Degrange. Dental Materials 25 (2009) 729-735.
[44] G. Zack, W. Rogers, S. Latt. Journal of Histochemistry & Cytochemistry 25 (1977) 741-753.
[45] J.G. Berryman. Journal of Applied Physics 57 (1985) 2374-2384.
[46] S.C. Blair, P.A. Berge, J.G. Berryman. Journal of Geophysical Research: Solid Earth 101 (1996) 20359-20375.
[47] R. Liu, S. Pathak, W.M. Mook, J.K. Baldwin, N. Mara, A. Antoniou. International Journal of Plasticity 98 (2017) 139-155.
[48] W.C. Oliver, G.M. Pharr. Journal of materials research 7 (1992) 1564-1583.
[49] M.F.d. Magalhães, R.A.N. Ferreira, P.A. Grossi, R.M.d. Andrade. Journal of Dentistry 36 (2008) 588-594.
[50] J. Kinney, M. Balooch, D. Haupt Jr, S. Marshall, G. Marshall Jr. Journal of dental research 74 (1995) 1179-1184.
[51] H. Deyhle, O. Bunk, B. Müller. Nanomedicine: Nanotechnology, Biology and Medicine 7 (2011) 694-701.
[52] W. Wang. Caractérisation géométrique et mécanique multi-échelle de la dentine humaine. Paris Saclay, 2016.
[53] L.E. Bertassoni, S. Habelitz, J.H. Kinney, S.J. Marshall, G.W. Marshall. Jr. Caries Research 43 (2009) 70-77.
[54] V.S. Deshpande, N.A. Fleck. Journal of the Mechanics and Physics of Solids 48 (2000) 1253-1283.
[55] L. Lührs, C. Soyarslan, J. Markmann, S. Bargmann, J. Weissmüller. Scripta Materialia 110 (2016) 65-69.
[56] Z. Hashin. Journal of Applied Mechanics 29 (1962) 143-150.
[57] C. Arson, Y. Yasothan, R. Jeanneret, N. Roubier, E. Vennat. Journal of Mechanics in Medicine and Biology (under review).
[58] J. Snyder, J. Erlebacher. ECS Transactions 41 (2011) 1021-1030.

[59] Z. Zhang, Y. Wang, Z. Qi, J. Lin, X. Bian. The Journal of Physical Chemistry C 113 (2009) 1308-1314.
[60] Y. Ding, J. Erlebacher. Journal of the American Chemical Society 125 (2003) 7772-7773.
[61] S. Gheorghiu, M.O. Coppens. AIChE journal 50 (2004) 812-820.

Figure(s)

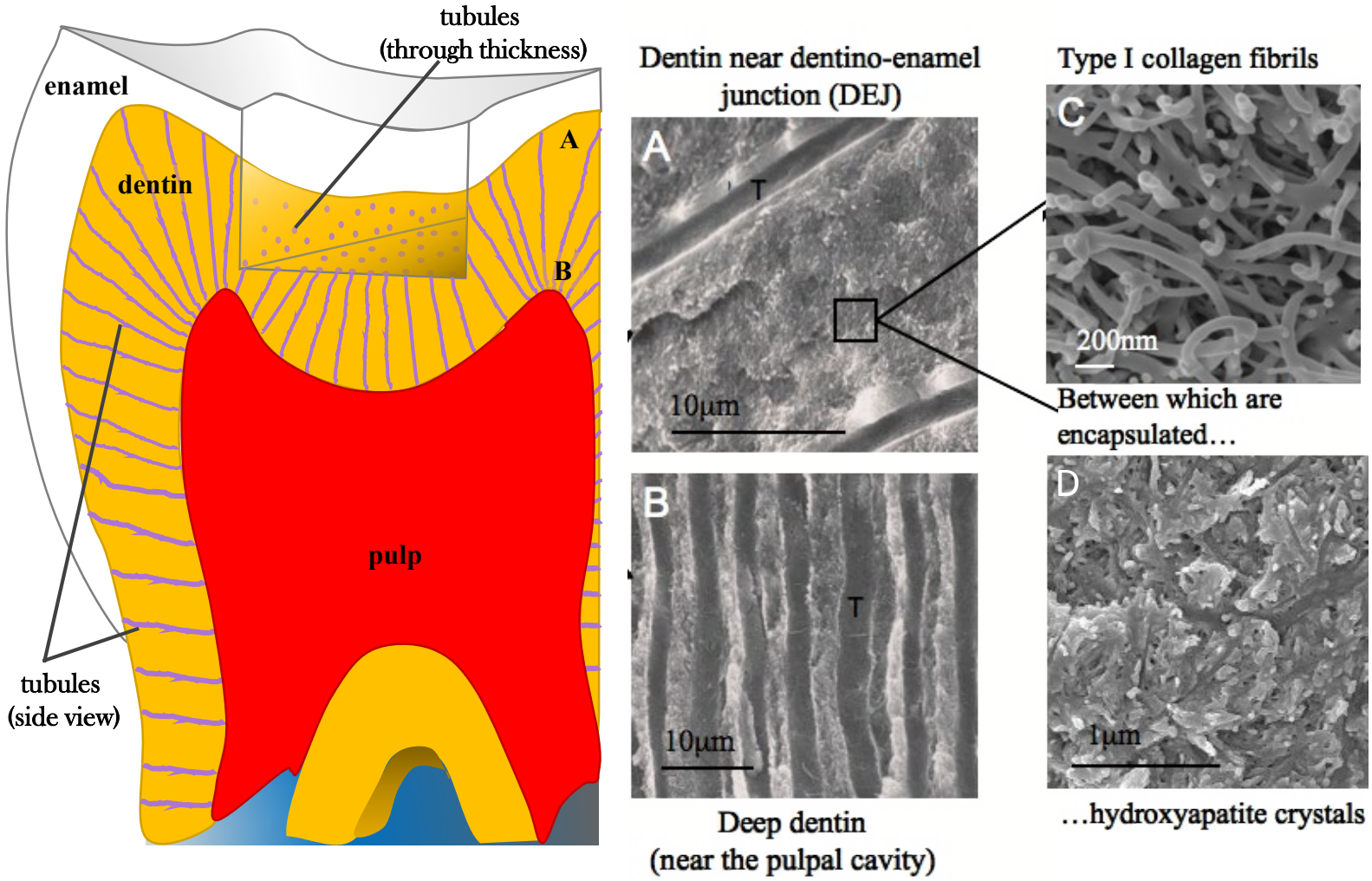

Figure 1. Schematic and SEM images depicting the main components of a tooth. The transverse isotropy induced by the presence of tubules is highlighted in the schematic, where tubules appear circular in the through thickness direction and longitudinal in the side view. SEM images show that tubules (T) closer to the enamel (A) are smaller in diameter and more sparsely distributed compared with tubules closer to the pulp (B). Dentin itself has a hierarchical structure consisting of (C) collagen fibers and (D) hydroxyapatite crystals.

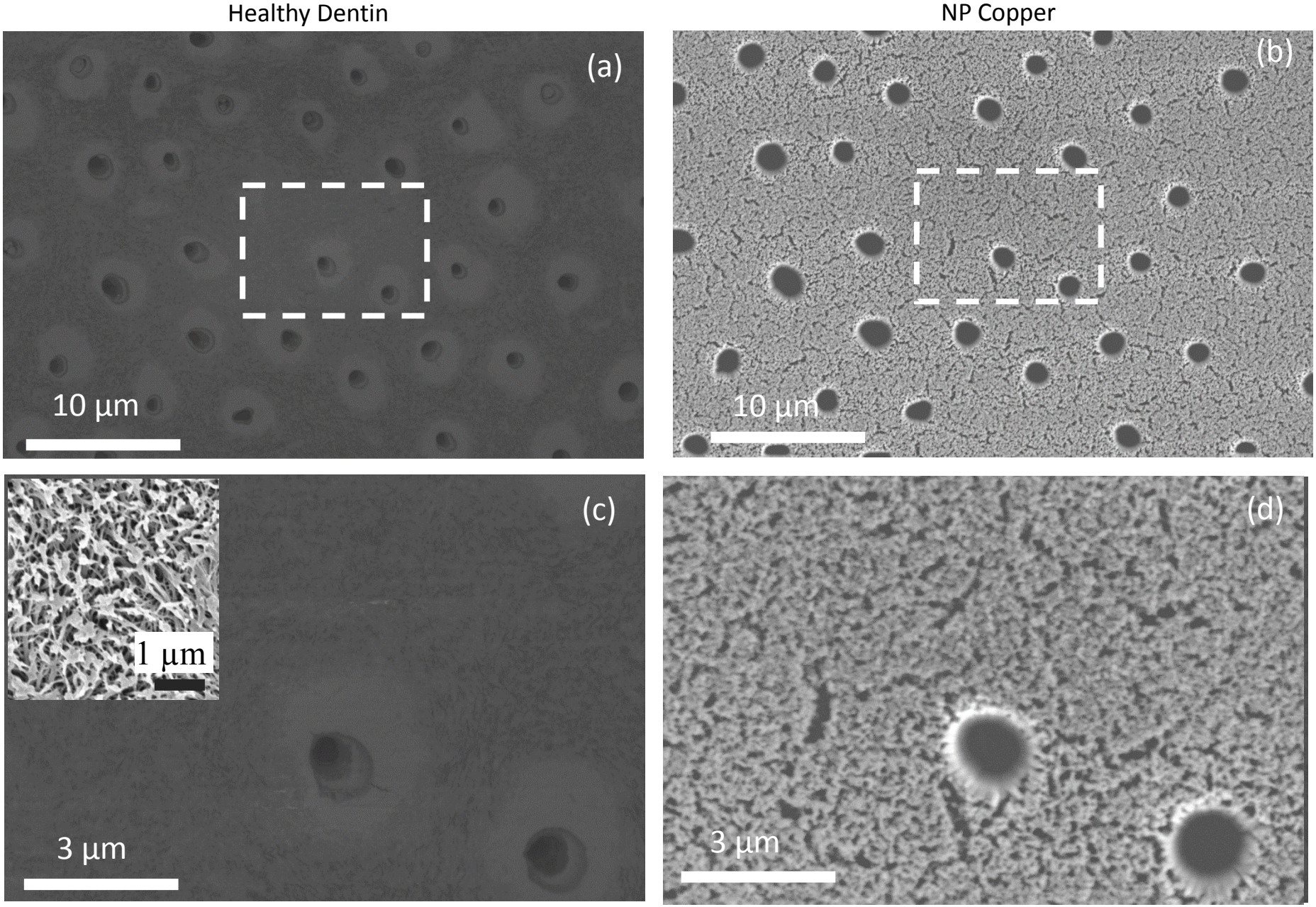

Figure 2. SEM plan view of (a) dentin tubules with (b) the corresponding tubule arrangement and spacing replicated in NP Copper. A close-up region around the tubules in (c) healthy dentin and the (d) replicated ones in NP Copper. The insert image in (c) shows the structure of dentin after the collagen is etched (demineralized dentin).

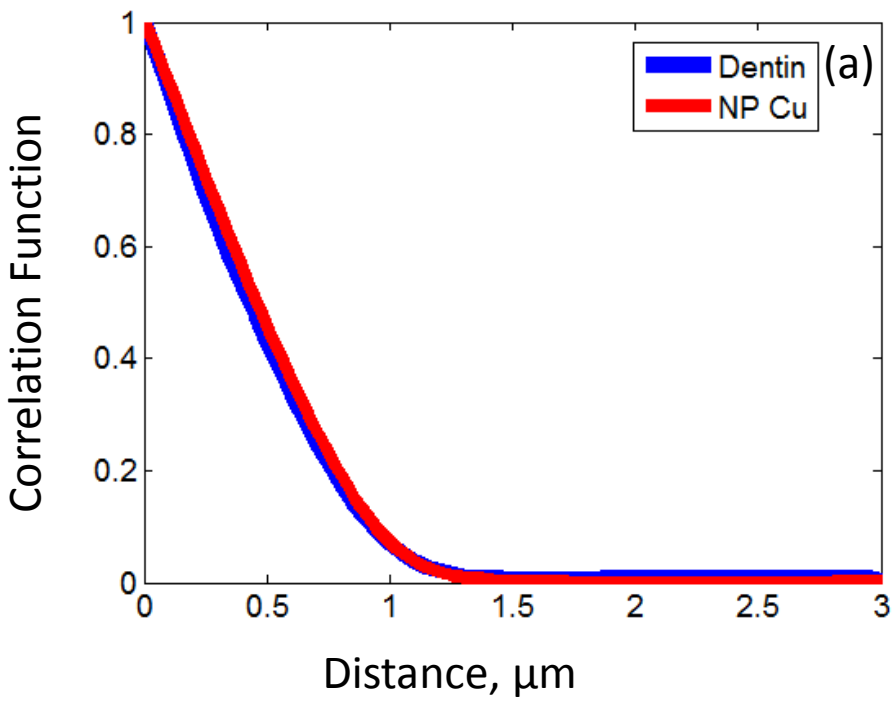

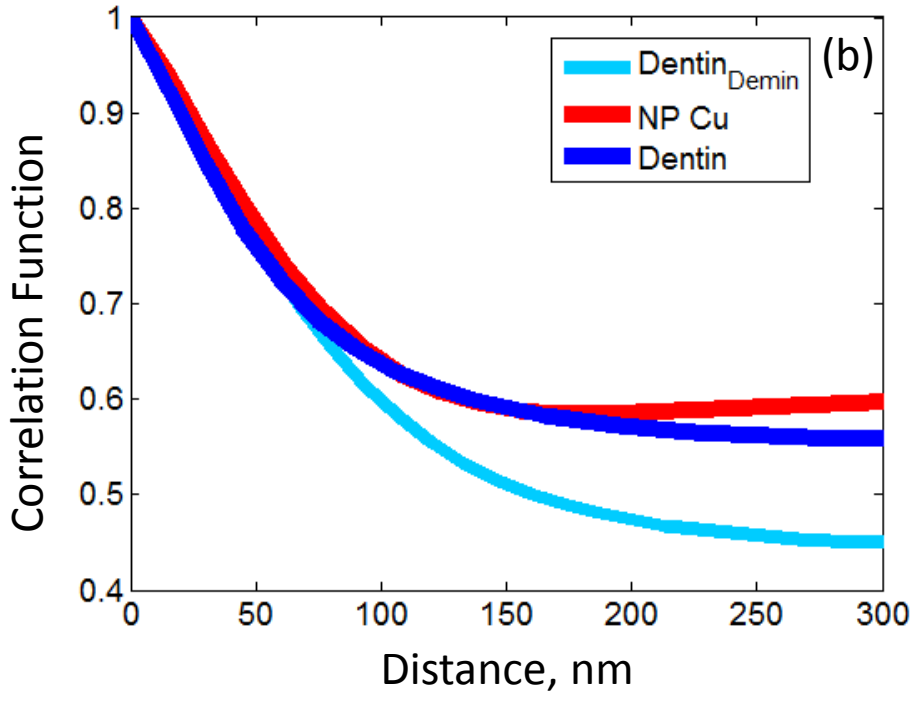

Figure 3. Two point correlation functions of pores (a) at the micron scale and (b) at the nano scale for both healthy dentin and NP Copper. The structure of demineralized dentin is also included in (b) the nanoscale.

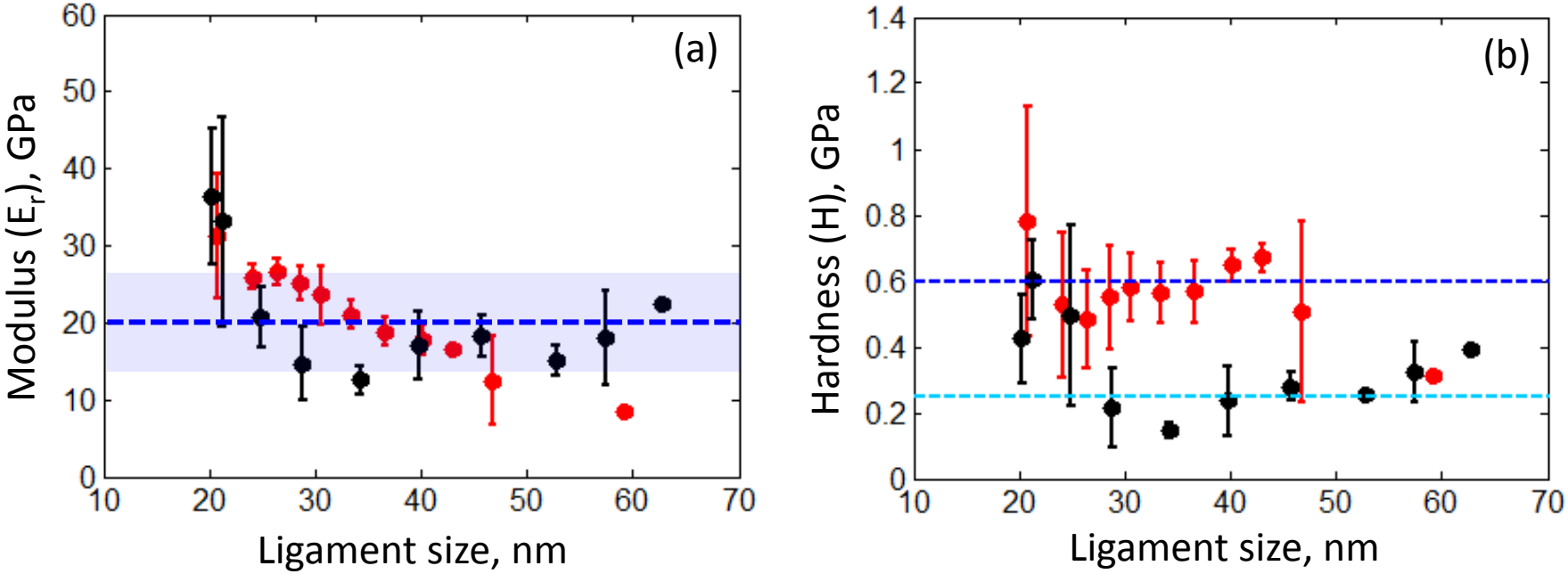

Figure 4. (a) Reduced modulus and (b) Hardness as a function of NP Copper ligament size, as assessed from Berkovich nanoindentation. Black symbols: NP Copper from Cu0.25Si0.75. Red circles: NP Cu from Cu0.41Si0.59. The dashed lines show the properties of healthy (blue) and demineralized dentin (cyan).

Table 1. Comparison of feature sizes and mechanical properties of dentin (healthy and demineralized) and NP Copper

Geometrical and Mechanical Properties	Dentin (D)	Demineralized dentin (DD)	Nanoporous Copper (NC)
Total porosity (%)	1-10 [21],[35],[61]	70-90 [62]	40-60% (tunable)
Average ligament size (nm)	5-50 (HA platelet size)	~100 (collagen fibril diameter)	18-80 (tunable)
Second order pore size (nm)	-	~100 [21]	30-100
First order pore size (tubule diameter) (µm)	1 (varies with location)	3 (corresponds to enlarged tubules and varies with location)	Can be fabricated with various techniques
Young's Modulus, E (GPa)	18-30 [61]	0.25 [63]	10-50 (tunable)
	~20 (ITD)	-	
	~30 (PTD)	-	
Plastic Poisson Ratio, v^P	0.3	-	0.2-0.3 [42]